Micro AUV Localization for Agile Navigation with Low-cost Acoustic Modems

Daniel A Duecker*, Fabian Steinmetz*, Edwin Kreuzer, and Christian Renner

***Abstract*—High-rate self-localization for agile navigation still constitutes a major bottleneck in micro autonomous underwater vehicle (μAUV) research. Hereby, key challenges arise from the system being small-size and low-cost, which excludes common approaches such as relying on sophisticated ring-laser gyroscopes. In this context, we investigate two promising sensor fusion strategies for μAUVs based on low-cost sensors and motion models. We benchmark our findings in experiments against a baseline linear least-square estimator and a GPS reference track.**

***Index Terms*—Underwater Localization, ahoi modem, acoustic ranging, micro AUV**

I. Introduction

The field of small-scale underwater robots has gained considerable research interest in recent years. In particular, the miniaturization of powerful and energy-efficient electronic components such as single board computers and flight controllers boosted the development of micro underwater vehicles.

Despite recent technological progress, accurate and robust self-localization constitutes a severe bottleneck when advancing autonomous capabilities of micro underwater robots. Full-scale robot platforms can supplement an unreliable localization signal with accurate data from advanced onboard inertial measurement units (IMU). Obviously, these high fidelity approaches contradict the idea of low-cost small-scale systems such as micro autonomous underwater vehicles (μAUVs). Note that this vehicle class is defined by a characteristic length-scale of less than 50 cm, see Fig. 1. Due to their tetherless design and their agile dynamics, μAUVs constitute a favorable solution for fully autonomous monitoring and inspection missions in confined and unstructured environments such as marinas. However, a high level of autonomy demands for accurate and reliable positioning.

The choice of the suitable localization technology is directly connected to the environment in which the micro underwater robot shall be deployed and its mission tasks to be conducted. Among others, key decision parameters are the dimensions of the environment, the required localization accuracy, and the visibility conditions. When optimizing for these parameters a trade-off arises as no underwater localization technology is ideal for all scenarios. High accuracy within small water tank dimensions has been demonstrated with μAUVs using electro-magnetic wave attenuation [1], [2]. However, this approach suffers from short ranges and high sensitivity against uncompensated orientations. Vision-based localization has been extensively studied throughout many robot domains and constitute a reliable choice for good visibility conditions. This can be expected in environments such as nuclear storage ponds or research tanks. These usually come with clear water and are thus attractive for vision-based approaches such as [3]–[5]. Indeed, good visibility conditions cannot be assumed for most outdoor deployments e. g. marinas, where turbidity limits the performance of visual localization

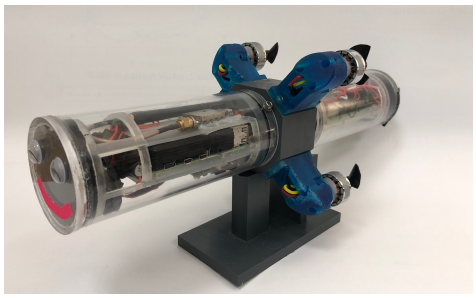

Fig. 1. HippoCampus μAUV with a total length of 45 cm [9], [10].

As by now, acoustic localization is the method of choice for these scenarios [6]. However, most of the localization systems come with high cost and complex infrastructure including e. g. including wired base stations. A widely used and relative low-cost system is the Waterlinked Underwater GPS [7], starting at €4500. The surface base unit calculates the position. However, the position signal has to be transmitted to the underwater robot first, before it can be used for feedback control. This is usually done via a tether cable, which contradicts the concept of fully autonomous and agile μAUV.

Therefore, this paper studies a methodology which enables localization independent from any connection to a base station. Our work uses the recently introduced *ahoi* acoustic modem which aims to be small, energy-efficient, and low-cost [8]. Hence, it constitutes a ideal fit for μAUV deployment. Furthermore, the ahoi modem is an open source licensed software and hardware project[1]. In sum, the ahoi modem comes with a price less than €600 per unit making acoustic localization systems available even to limited budgets.

* Authors contributed equally. All authors are affiliated with TU Hamburg, Germany. Please direct correspondence to {daniel.duecker, fabian.steinmetz}@tuhh.de. This research was supported by the German Research Foundation (DFG) under grant Kr 752/36-1, the German Federal Ministry for Economic Affairs and Energy (BMWi, FKZ 03SX463C), and ERA-NET Cofund MarTERA (contract 728053)

[1] http://www.ahoi-modem.de/

Contribution

In this work, we study the problem of self-localization for agile navigation with μAUVs in a confined marina environment based on a low-cost acoustic modem. So far, agile navigation of μAUVs is often hindered by the low-frequent absolute position information its sensitivity to position measurement outages. Therefore, in the context of *low-cost* μAUVs, we investigate promising strategies to improve update rate and accuracy. Namely, we propose a Kalman filter based sensor fusion architecture to identify robustness and accuracy gains due to

- time-compensated sequential measurement updates, and
- μAUV motion models.

We benchmark our findings against a baseline linear least-squares (LLS) estimator and GPS in real-world experiments.

II. Background

Underwater localization is a challenging task. Due to the high damping of the electro-magnetic wave in the water, most over-water systems such as global positioning system (GPS) or other global navigation satellite system (GNSS) are not available. Furthermore, optical systems are non-applicable as a result of the poor visibility in many areas. During the past decades, many researchers developed solutions for underwater localization. The authors in [6] give an excellent overview over different systems.

As an example for a system without any additional requirements (outside of the μAUV), is a localization based on dead-reckoning. The authors in [11] used a combination of a GPS, a doppler velocity log (DVL), an altitude, and pressure sensor to calculate the vehicle position. From time to time, the AUV surfaces and determines its position via GPS. During the mission in between the GPS fixes, the AUV calculates the position based on the its estimated rotation, depth, and velocity. Indeed, this requires high-fidelity sensors, which are expensive compared to the cost of an μAUV.

Another approach is to localize the μAUV with distance measurements to external reference stations. More details provide the following surveys [6], [12]. Figure 2 shows different acoustic localization approaches. In all cases, the μAUV carries a transmitter, which periodically emits acoustic beacons. The receivers are installed at fixed positions and receive the beacons. Knowing the speed of sound, the distances between transmitter and receivers can be calculated based on the travel time of the acoustic signal. Long baseline (LBL) systems cover a wide area and the receiver are mounted on fixed structures in the underwater environment, e. g., the seabed. Opposed to that, in short baseline (SBL) systems the receivers are mounted with smaller distances to one another, e. g., at the outer edges of a ship hull or under buoys within a restricted area. In ultra-short baseline (USBL) systems, multiple hydrophones or receivers are arranged as an array at a single position, e. g., at the center of a boat. The systems in Fig. 2b and Fig. 2c calculate the relative position between boat and μAUV. In order to receive the position in global coordinates, an additional absolute reference system (e. g., GPS) is required to determine the boat absolute position. Typical distances between the receivers range from $50\,\mathrm{m}$ to more than $2000\,\mathrm{m}$ for LBL systems, from $20\,\mathrm{m}$ to $50\,\mathrm{m}$ for SBL systems, and less than $10\,\mathrm{cm}$ for USBL systems [12].

The described baseline systems come with several disadvantages, which hamper the utilization in μAUVs:

- Baseline systems calculate the μAUV location at the receiver side. In many applications, e. g., autonomous navigation, the control unit on the μAUV requires the vehicle's current absolute position. For these cases, the position must be sent to the μAUV via an additional communication system.
- The receivers must be synchronized, which requires accurate and expensive oscillators. Note that in approach approaches this also yields for transmitter side. For example, the authors in [13] use chip scale atomic clocks (CSAC) to synchronize their localization system.
- Commercial systems are expensive compared to the price of μAUVs. For example, Subsonus USBL/INS produced by Advanced Navigation starts at €20 000 for an USBL receiver [14]. Another example is the Underwater GPS by Water Linked AS [7], which is a SBL system suggested from Blue Robotics Inc. for the BlueROV2. Note the whole BlueROV2 platform with minimal configuration starts at €3500 [15], while the Underwater GPS settles at circa €4500.
- In general, baseline systems do not enable a communication link between μAUV and reference station. However, some commercial systems offer piggybacked communication.

III. Underwater Ranging

In the following, we briefly present the fundamentals on acoustic underwater ranging and its application to localization..

A. ahoi Modem

The ahoi modem is a small, low-power and low-cost acoustic underwater modem [8]. The modem was developed for the integration into μAUVs as well as underwater wireless sensor networks (UWSNs). The basic design consists of stacked printed circuit boards (PCBs) (size of $50 \times 50 \times 25\,\mathrm{mm}^3$) and an external hydrophone, see Fig. 1. The price of a single ahoi modem is circa €600, consists of €200 for PCBs and component costs and €400 for the hydrophone. In this paper, we used well-known and already tested hydrophones. However, it is possible to connect cheaper hydrophones to the ahoi modem. In the default setup, the ahoi modem has a net data rate of $260\,\mathrm{bit/s}$. In previous evaluations, the modem was tested over communication ranges above $150\,\mathrm{m}$.

B. TWR-based Ranging

In addition to the regular packet-based communication, the ahoi modem provides a two-way ranging (TWR)-based distance estimation between two modems. In general, the first

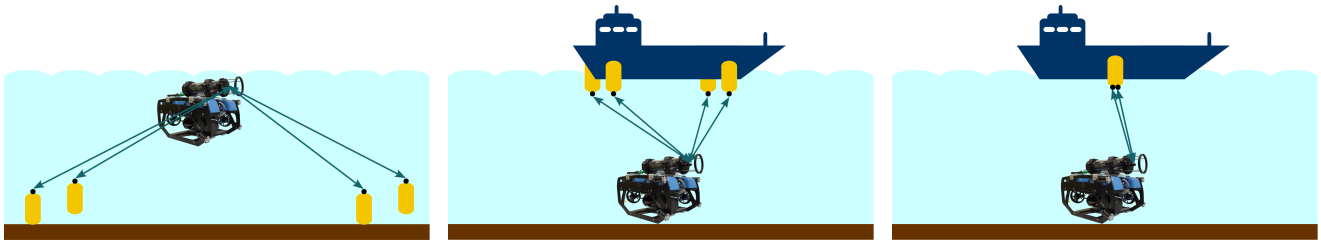

(a) LBL system (b) SBL system (c) USBL system

Fig. 2. Acoustic underwater localization systems. The μAUV (in these figures a BlueROV2) carries a transmitter to localized the μAUV with distance measurements to receivers (in yellow) at fixed positions.

Fig. 3. ahoi modem with hydrophone

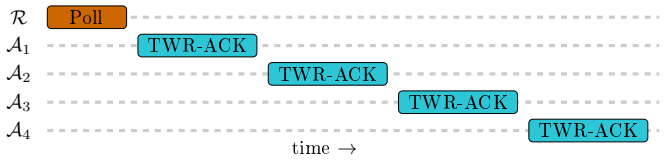

Fig. 4. Ranging round with agent or robot $\mathcal{R}$ and anchors $\mathcal{A}_1$ to $\mathcal{A}_4$. The agent initializes the cycle with a poll packet and the anchors reply (TWR-ACK) with different delays to avoid packet collisions.

modem initiates the TWR with a short poll, transmitted to the second modem. The second modem replies an acknowledgment (ACK). After receiving the ACK, the first modem estimates the propagation time of the acoustic wave. Based on the maximal communication range, as discussed in Sect. III-A, the TWR-based ranging is capable of measuring distances up to $150\,\mathrm{m}$. We refer the reader to [16] for a more detailed description.

C. TWR-based Localization

In order to enable a TWR-based localization, the described setup in Sect. III-B can be extended. An agent or robot $\mathcal{R}$ (e. g., a μAUV) initializes the process with a broadcast poll packet to multiple anchors. In this example, the agent transmit a packet to the anchors $\mathcal{A}_1$ to $\mathcal{A}_4$. To avoid packet collisions, the anchors responses sequentially after a predefined delay time, as illustrated in Fig. 4. At first, agent $\mathcal{R}$ transmits the poll packet (length T_{poll}). Anchor $\mathcal{A}_1$ replies with an ACK direct after the reception of the poll. Opposed to that, anchor $\mathcal{A}_2$ waits for a delay T_{del} and replies afterwards. Note that the delay T_{del} is chosen longer than T_{ack} and the maximal propagation time (in this setup). The subsequent anchors $\mathcal{A}_3$ and $\mathcal{A}_4$ proceed in the same way and wait for $2 \cdot T_{\text{del}}$ respectively $3 \cdot T_{\text{del}}$. The reader is referred to [17] for an investigation on the accuracy of TWR-based ranging.

The setup is not limited to a configuration of four anchors. However, the frequency of the polling packets decreases with an increasing number of anchors. Finally, given successful ACK receptions, the agent can compute its position based on the measured ranges and fixed and known positions of the anchors.

The TWR-based localization system can be used as a LBL or SBL system. Opposed to the discussed disadvantages at the end of Sect. II the μAUV receives the distances, which enables a self-localization on the vehicle. Note that TWR-ranging naturally does not require synchronized clocks. In addition, the ranging capability is piggybacked on the communication layer of the ahoi modem. Based on that, it is possible to use the same system to exchange data between the μAUV and the anchor modems and the optional notebook base station. Indeed, it comes with a some cost. From the data communication point of view, the ranging reduces the channel capability with respect to the data throughput. On the other hand, a data communication reduces the ranging frequency.

Furthermore, the position update rate depends on the number of anchors. For example, with four ahoi modem anchors and without data communication, the polling packet interval is in between $3\,\mathrm{s}$ to $5\,\mathrm{s}$ ($0.33\,\mathrm{Hz}$ down to $0.2\,\mathrm{Hz}$). Opposed to that, commercial SBL or USBL systems have higher position update rates, e. g., the Underwater GPS provides up to $4\,\mathrm{Hz}$ [7] and the Subsonus USBL/INS up to $10\,\mathrm{Hz}$ [14].

IV. Self-Localization for Agile Navigation

We derive a self-localization scheme based on TWR.

Let ${}^{\mathcal{W}}\boldsymbol{p}_k$ describe the state of an agent $\mathcal{R}$ in a world-fixed reference frame $\mathcal{W}$ at time step k,

$$ {}^{\mathcal{W}}\boldsymbol{p}_k = \left[x, y, z, \dot{x}, \dot{y}, \dot{z}\right]^\top , \tag{1}$$

defining its position and the corresponding translational velocities respectively.

Moreover, we define the distance between agent $\mathcal{R}$ and i^{th}-anchor position ${}^{\mathcal{W}}\boldsymbol{p}_{\mathcal{A}_i}$ as d_i^{3D}, measured in 3D space including the depth component

$$ d_i^{\text{3D}} = \sqrt{{}^{\mathcal{W}}\boldsymbol{p}_k^2 - {}^{\mathcal{W}}\boldsymbol{p}_{\mathcal{A}_i}^2}. \tag{2}$$

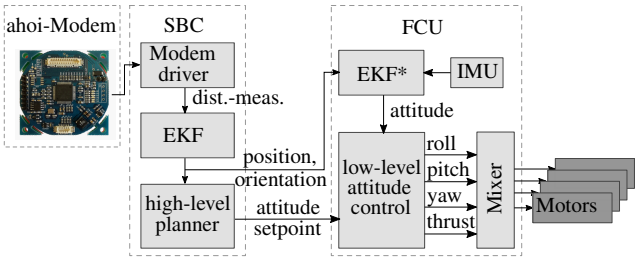

Fig. 5. Architecture of the acoustic self-localization scheme for μAUVs

A. Architecture

In order to achieve a high modularity of the acoustic localization system, we propose a loosely-coupled implementation onboard a single board computer (SBC) which is connected with the agent's flight control unit (FCU) as depicted in Fig. 5. The modem driver is implemented on the SBC and communicates with the ahoi modem. It computes the anchor-agent distance measurement based on given environmental parameters such as speed of sound and salinity. These distances are then fed into the EKF, described in detail in Sect. IV-B. The estimated agent's absolute position is then send to the FCU's EKF (EKF*) which fuses onboard IMU data and compensates for additional latencies. Moreover, the FCU runs the time critical low-level controller with computes the required motor commands.

B. Extended Kalman Filter

Simple localization algorithms such as the linear least squares (LLS) usually come with various drawbacks. Namely, multiple measurements have to be temporarily stored before the position can be calculated and the unavailability of position information in between the measurement update steps. Moreover, they do not provide a measure on the quality of the calculated position. We target these flaws with an extended Kalman filter (EKF) scheme which sequentially incorporates the incoming TWR measurements. This allows in combination with a robot motion model and onboard IMU data to compensate for measurement latencies. Moreover, the EKF-prediction provides high-rate inter-measurement position information resulting in more reliable information for the robot controller.

The predicted state and its covariance read

$$\hat{\boldsymbol{p}}^{(-)}(k) = \boldsymbol{f}\left(\hat{\boldsymbol{p}}^{(+)}(k-1)\right) \quad \text{and} \tag{3}$$

$$\hat{\boldsymbol{P}}^{(-)}(k) = \boldsymbol{F}\hat{\boldsymbol{P}}^{(+)}(k-1)\boldsymbol{F}^{\top} + \boldsymbol{Q}, \tag{4}$$

where $\boldsymbol{f}$ is the agent motion model and $\boldsymbol{F}$ its linear form. Moreover, $\boldsymbol{Q}$ represents the corresponding process noise matrix in diagonal form. The superscripts (-) and (+) indicate values gained before and after incorporating the measurement μ respectively. Note that for the sake of simplicity we favor a general motion model. Based on our experience from early experimental trials, we find a linear particle model sufficient to describe the agent dynamics. More complex models are of course possible and can be easily implemented.

The state update is based on the measurement $\boldsymbol{\mu}$ which is modeled by the nonlinear observation function $\boldsymbol{h}(\boldsymbol{p})$. It consists of the distances d_i between the robot and the anchors $\mathcal{A}_i$ which are located at known positions. For the sake of simplicity, we assume from now on a common configuration consisting of $N = 4$ anchors. Note that in the case of a polling cycle resulting in zero received measurement, e. g. due to package losses, the Kalman update step is skipped and the algorithm continues. The single robot-anchor measurement yields

$$\mu_{k,i} = h_i(\boldsymbol{p}_k) = \sqrt{{}^{\mathcal{W}}\boldsymbol{p}_k^2 - {}^{\mathcal{W}}\boldsymbol{p}_{\mathcal{A}_i}^2},$$

as stated in Eq. (2). Thus, the measurement vector $\boldsymbol{\mu}$ consisting of up n received distance measurements yields

$$\boldsymbol{\mu}_k = \left[\mu_{k\,\mathcal{A}_1} \cdots \mu_{k\,\mathcal{A}_n}\right]. \tag{5}$$

Thus, the corresponding Jacobian matrix has the form

$$\boldsymbol{J}_{\boldsymbol{p}(k)} = \left[\nabla_{\boldsymbol{p}(k)} h_1(\boldsymbol{p}(k))^{\top} \cdots \nabla_{\boldsymbol{p}(k)} h_N(\boldsymbol{p}(k))^{\top}\right]^{\top}. \tag{6}$$

Note that the dimensions of μ and thus $\boldsymbol{J}$ change dynamically with the number of received range measurements in each measurement cycle. For the general case of sequentially received and processed measurements we directly fuse the measurements as they arrive.

In order to update the estimated state based on the measurement $\boldsymbol{\mu}$ the Kalman-gain reads

$$\boldsymbol{K}(k) = \hat{\boldsymbol{P}}^{(-)}(k)\boldsymbol{J}_{\boldsymbol{p}(k)}\left(\boldsymbol{J}_{\boldsymbol{p}(k)}\hat{\boldsymbol{P}}^{(-)}(k)\boldsymbol{J}_{\boldsymbol{p}(k)}^{\top} + \boldsymbol{R}\right)^{-1} \tag{7}$$

where $\boldsymbol{R}$ is the measurement noise.

Thus, the state update yields

$$\hat{\boldsymbol{p}}^{(+)}(k) = \hat{\boldsymbol{p}}^{(-)}(k) + \boldsymbol{K}(k)\left(\boldsymbol{\mu}(k) - \boldsymbol{h}(\hat{\boldsymbol{p}}^{(-)}(k))\right), \tag{8}$$

$$\hat{\boldsymbol{P}}^{(+)}(k) = \left(\boldsymbol{I} - \boldsymbol{K}(k)\boldsymbol{J}_{\boldsymbol{p}(k)}\right)\hat{\boldsymbol{P}}^{(-)}(k). \tag{9}$$

Note that we compensate for individual time stamp shifts. Due to the time required for packet polls and anchor reply the filter algorithm runs on a delayed fusion horizon.

C. LLS-Baseline

The LLS-method was previously used in [8] to calculate the μAUV position. This procedure is straight forward and directly results into a position estimate. Therefore, it is used as a benchmarking baseline for our previously described EKF-algorithm. However, LLS concept naturally ignores different arrival times of the individual measurements. In the following, the LLS method is used as benchmark and for comparison to EKF.

In most scenarios, the agent and anchor depths can be measured directly with pressure sensor and are thus accurately known. Hence, localization can be converted to a 2D system with d_i^{2D} denoting distance between agent and anchor

$$d_i^{\mathrm{2D}} = \sqrt{\left(d_i^{\mathrm{3D}}\right)^2 - \left(z_{\mathcal{R}} - z_i\right)^2}, \tag{10}$$

(a) BlueROV2 (B) and attached GPS receiver (G)

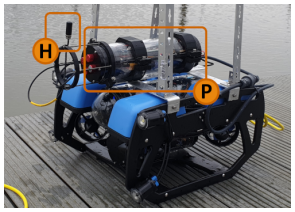

(b) Hydrophone (H), additional tube respectively payload (P)

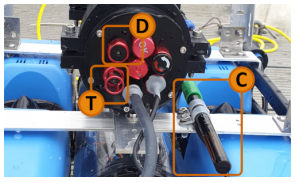

(c) Temperature (T), pressure or depth (D) and salinity or conductivity (C) sensors

Fig. 6. BlueROV2 configuration and additional GPS receiver. This setup was used for the real-world evaluation.

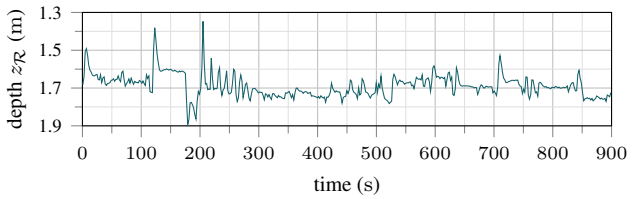

Fig. 7. BlueROV2 depth profile during the real-world evaluation.

with the agent depth $z_\mathcal{R}$ and i^{th}-anchor depth z_i.

Each TWR cycle, the received distances are converted into the 2D plane. When the agent receives more than three distance measurements out of one cycle, the position is calculated with the implementation provided by [18].

However, in the case of a communication high packet loss this implementation result in a poor position update rate.

V. Analysis

The experimental evaluation took place in a small marina in Finkenwerder in Hamburg, Germany (February 2020). The confined evaluation area was already used for previous localization experiments, which were published in [8]. During the evaluation, the received packets, GPS positions, and vehicle data were recorded, which allows a post-processing with various localization algorithms, namely the EKF-approach presented in Sect. IV-B and a linear least squares algorithm.

A. Experimental Setup

Four fixed reference points (anchors) denoted by $\mathcal{A}_1$ to $\mathcal{A}_4$ were installed on the marina's jetties as shown in Fig. 8a. Their positions are listed in Table I. The anchors' hydrophones were mounted submerged at $1.5\,\text{m}$ depth.

All necessary localization components fit into the small μAUV HippoCampus. However, for this special examination we deploy the fifth ahoi modem on a BlueROV2 as this platform is capable of carrying an additional rig, see Fig. 8a. This

TABLE I
Anchor Positions

	$\mathcal{A}_1$	$\mathcal{A}_2$	$\mathcal{A}_3$	$\mathcal{A}_4$
x	42.17 m	18.15 m	−24.25 m	0 m
y	26.65 m	64.18 m	37.63 m	0 m
z	1.50 m	1.50 m	1.50 m	1.50 m

allows to record a GPS-reference track during the experiment. Therefore, a $2\,\text{m}$ rig was mounted on top of the BlueROV2 which kept the GPS receiver above water level while the robot could remain submerged at $1.5\,\text{m}$ depth,see Fig. 6a. We used a Navilock NL-8001U GPS receiver with a position accuracy of $2.5\,\text{m}$ circular error probable (CEP) [19].

We installed the ahoi modem in an additional tube on top of the BlueROV2, as shown in Fig. 6b. The hydrophone was placed in front of the tube to achieve an omnidirectional sensitivity. During the evaluation, the recorded distance measurements are with respect to the hydrophone. In addition to the modem, the tube houses a Raspberry Pi Zero, a power supply and conductivity temperature depth (CTD) sensors. Depth measurements $z_\mathcal{R}$ were provided by an onboard pressure sensor. The recorded depth track is depicted in Fig. 7.

Note that the speed of sound depends on depth, temperature, and salinity [20]. Therefore, we chose an integrated sensor suite which enables a self-estimation of the speed of sound within the operating area.

However, in order to determine a reference value for the speed of sound, we additionally used a professional CTD probe, which measured a water temperature of $5.0\,^\circ\text{C}$ and $0.47\,\text{ppt}$ salinity at a depth of $1.3\,\text{m}$. Based on that, the speed of sound was $1427\,\text{m/s}$.

During the evaluation, the agent (BlueROV2) transmitted a poll packet ($T_\text{poll} = 820\,\text{ms}$) every $3.5\,\text{s}$. The poll packet includes $16\,\text{B}$ random payload, which we block to simulate transmitted information from the μAUV to the anchors. This way, the anchor can be used a relay station to an over water network. The ACK had a length of $T_\text{ack} = 451\,\text{ms}$ and the response delays were adjusted to $T_\text{del} \in \{0\,\text{s}, 0.7\,\text{s}, 1.4\,\text{s}, 2.1\,\text{s}\}$ (anchor $\mathcal{A}_1$ to $\mathcal{A}_4$).

B. Robot Self-Localization

In the following, we evaluate the localization performance of our EKF self-localization algorithm from Sect. IV-B in comparison to the LLS-baseline and the GPS-reference path which was recorded during the trials.

Therefore, we drove the agent with a speed of ca. 0.5 m/s along the path and travelled two cycles. The first lap from $0\,\text{s}$ to $400\,\text{s}$ and the second from $400\,\text{s}$ to $900\,\text{s}$. Figure 8 depicts the second lap. The total path length of two laps was about 281 m based on the recorded GPS data. During the experiments the agent aims to continuously hold a depth of 1.5 m. The agent's depth profile is depicted in Fig. 7.

During the evaluation ($900\,\text{s}$ long), the agent transmitted 255 poll packets and received 249 ACKs from anchor $\mathcal{A}_1$ ($97.7\,\%$ received ACKs), 250 ACKs from $\mathcal{A}_2$ ($98.0\,\%$),

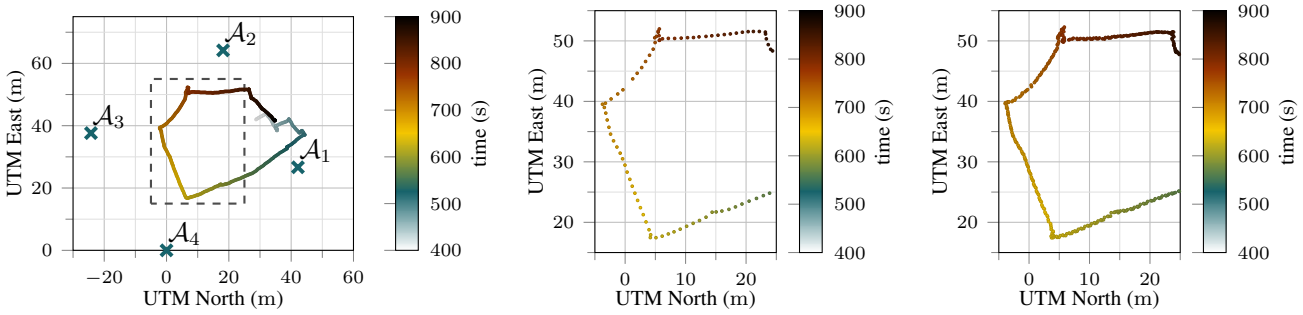

(a) GPS track (agent $\mathcal{R}$) and anchor positions. (b) LLS-based localization (c) EKF-based localization

Fig. 8. Localization setup and comparison between two algorithms (second lap between 400 s to 900 s). The first figure depicts the positions of the anchors $\mathcal{A}_1$ to $\mathcal{A}_4$ and the recorded GPS track of the agent $\mathcal{R}$. Figures 8b and 8c show a part of the area (dashed rectangle in Fig. 8a) and compare the EKF and LLS localization algorithms. In all cases, UTM coordinates (grid zone 32U) were used, normalized relative to the position of anchor $\mathcal{A}_4$.

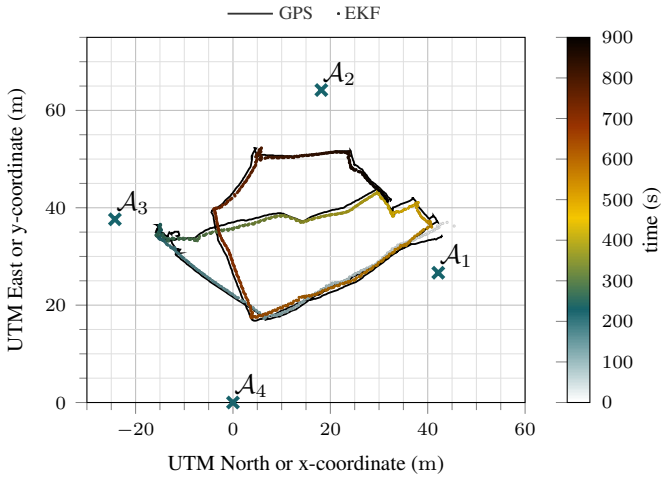

Fig. 9. EKF and GPS tracks over two laps.

247 ACKs from $\mathcal{A}_3$ (96.7 %), and 249 ACKs from $\mathcal{A}_4$ (97.7 %).

As can be seen in Fig. 8 both, the LLS and the EKF path shape match accurately with the GPS-reference path. Note that we identified a constant offset of 2.3 m in negative x-direction in the original data set. This could be observed throughout the trial and is likely due to the GPS distortion, given the GPS receivers accuracy [19]. For the sake of convenient comparison, we compensate our data by this constant offset.

As discussed in Sect. IV-C, the LLS algorithm computes the agent position at the end of the polling cycle after at least three distance measurements have been received by the agent. Generally, LLS is very sensitive to package losses which can result in a rejection of the whole polling cycle, if not a sufficient number of the cycle's distance measurements are received by the agent's modem. This constitutes a considerable drawback of the LLS approach. However, during our trials we recorded a dataset with a noticeable high PRR in comparison to experiments in earlier works [8], [21]. Thus, the LLS-localization can be performed in almost all polling cycles leading to an average position update of almost every 3.5 s which is close optimal given the used polling sequence described above. Note that the anchor-agent distances are measured sequentially. This naturally leads to a localization error, since the agents proceeds along its path during the measurement sequence.

In contrast, our EKF scheme fuses the individual anchor distance measurements immediately as they are received by the agent's modem. This is advantageous as no measurements representing *old* agent positions from previous time instances are fused into the position estimate. Note that the EKF-prediction step propagates the agent position for the time instance when the distance measurement is received. As a positive effect, this leads to a more continuous measurement update of the agent position, as can be seen in Fig. 8.

The agent's position profile over time is depicted in Fig. 10c. The estimated paths match accurately with the recorded GPS track.

Moreover, due to its motions model the EKF is able to estimate the agent velocity. The corresponding velocity time profiles are depicted in Fig. 11. As a reference we plot the GPS-velocity reconstructed from the GPS-position data points. We can observe that the EKF velocity estimate matches the GPS-velocity. However, the underlying EKF-motion model increases the robustness and provides a smooth estimate on the velocity's $x-$ and $y-$component. Note that accurate and smooth velocity information are a key requirement when predicting position estimates between the anchor distance measurements.

VI. Conclusion and Future Work

In this work we presented a low-cost approach to the problem of agile navigation based on a acoustic localization. Therefore, we combined the small scale ahoi acoustic modem with an extended Kalman Filter. The filter algorithm sequentially fuses anchor-agent distance measurements and compensates for time delays. We benchmarked our localization scheme against GPS reference data and a linear least squares localization method on real-world experiment data recorded in a marina using a small-scale underwater robot. As a result, we could demonstrate the accurate and robust localization performance of our method.

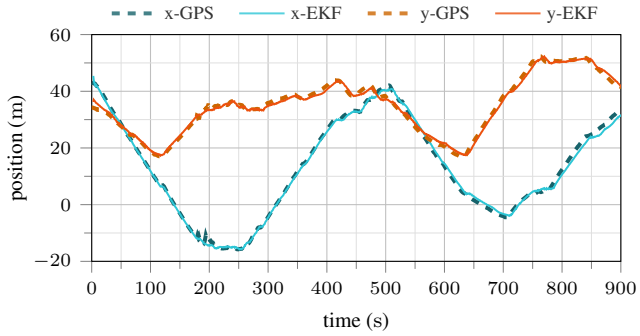

Fig. 10. GPS and EKF position profiles (x- and y-coordinates) of the BlueROV2 during real-world evaluation.

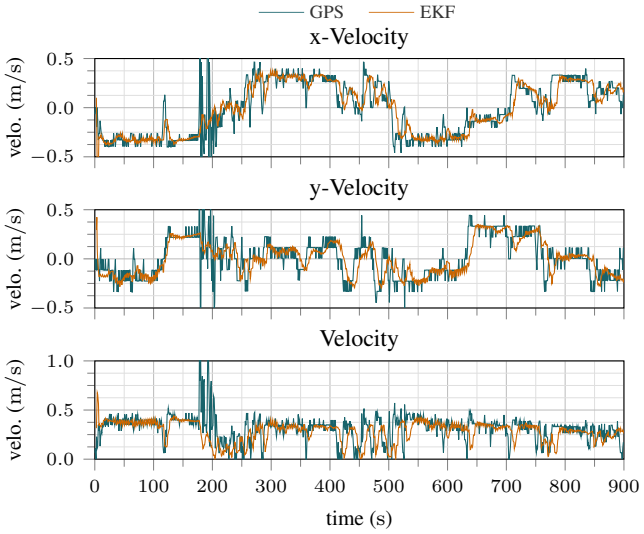

Fig. 11. GPS and EKF velocity profiles of the underwater robot over two laps.

However, our promising results constitute a first step and motivate further investigation of localization and control performance requirements during agile navigation tasks. Moreover, we will investigate the tracking behavior in the path's corner-cases and the sensitivity to reduced ranging-rates to enable a data communication beside the TWR.

References

[1] D. A. Duecker, A. R. Geist, M. Hengeler, E. Kreuzer, M. A. Pick, V. Rausch, and E. Solowjow, "Embedded spherical localization for micro underwater vehicles based on attenuation of electro-magnetic carrier signals," *Sensors (Switzerland)*, vol. 17, no. 5, 2017.

[2] D. A. Duecker, T. Johannink, E. Kreuzer, V. Rausch, and E. Solowjow, "An Integrated Approach to Navigation and Control in Micro Underwater Robotics using Radio-Frequency Localization," in *IEEE International Conference on Robotics and Automation (ICRA)*. Montreal: IEEE, 2019, pp. 6846–6852.

[3] E. H. Henriksen, I. Schjølberg, and T. B. Gjersvik, "Vision Based Localization for Subsea Intervention," in *Proceedings of the ASME 2017 36th International Conference on Offshore Mechanics and Arctic Engineering (OMAE)*, Trondheim, 2017, pp. 1–9.

[4] J. Jung, J. H. Li, H. T. Choi, and H. Myung, "Localization of AUVs using visual information of underwater structures and artificial landmarks," *Intelligent Service Robotics*, vol. 10, no. 1, pp. 67–76, 2017.

[5] D. A. Duecker, N. Bauschmann, T. Hansen, E. Kreuzer, and R. Seifried, "Towards Micro Robot Hydrobatics: Vision-based Guidance, Navigation, and Control for Agile Underwater Vehicles in Confined Environments," in *accepted at IEEE/RSJ International Conference on Intelligent Robots and Systems (IROS)*, Las Vegas, 2020.

[6] J. González-García, A. Gómez-Espinosa, E. Cuan-Urquizo, L. G. García-Valdovinos, T. Salgado-Jiménez, and J. A. E. Cabello, "Autonomous Underwater Vehicles: Localization, Navigation, and Communication for Collaborative Missions," *Applied Sciences*, vol. 10, p. 1256, 02 2020.

[7] Water Linked AS, "WL-11001 Underwater GPS Explorer Kit," https://waterlinked.com/underwater-gps/, 2018, accessed: 2020/05/25.

[8] C. Renner, J. Heitmann, and F. Steinmetz, "ahoi: Inexpensive, Low-Power Communication and Localization for Underwater Sensor Networks and µAUVs," *Transactions on Sensor Networks (TOSN)*, vol. 16, 2020.

[9] D. A. Duecker, N. Bauschmann, T. Hansen, E. Kreuzer, and R. Seifried, "HippoCampus X – A hydrobatic open-source micro AUV for confined environments," in *(accepted at) 2020 IEEE/OES Autonomous Underwater Vehicle Symposium (AUV)*, St. Johns, 2020.

[10] D. A. Duecker, E. Solowjow, and A. Hackbarth, "HippoCampus Robotics - An Open-Source Micro Underwater Robot Platform," 2020. [Online]. Available: HippoCampusRobotics.github.io

[11] H. C. Woithe, D. Boehm, and U. Kremer, "Improving Slocum Glider dead reckoning using a Doppler Velocity Log," in *MTS/IEEE OCEANS Conference & Exposition (OCEANS)*, Waikoloa, HI, USA, Sep. 2011.

[12] H.-P. Tan, R. Diamant, W. K. Seah, and M. Waldmeyer, "A survey of techniques and challenges in underwater localization," *Ocean Engineering*, vol. 38, no. 14, pp. 1663 – 1676, 2011.

[13] V. Djapic, W. Dong, D. Spaccini, G. Cario, A. Casavola, P. Gjanci, M. Lupia, and C. Petrioli, "Cooperation of coordinated teams of Autonomous Underwater Vehicles," in *9th IFAC Symposium on Intelligent Autonomous Vehicles (IAV)*, Leipzig, Germany, Jun. 2016, pp. 1–6.

[14] Advanced Navigation, "Subsonus USBL/INS Datasheet," https://www.advancednavigation.com/sites/default/files/product_documents/Subsonus_Datasheet_0.pdf, 2019, accessed: 2020/05/25.

[15] Blue Robotics Inc., "BlueROV2," https://bluerobotics.com/store/rov/bluerov2/, 2020, accessed: 2020/08/26.

[16] C. Renner, "Packet-Based Ranging with a Low-Power, Low-Cost Acoustic Modem for Micro AUVs," in *11th International ITG Conference on Systems, Communications and Coding*, ser. SCC '17. Hamburg, Germany: VDE, Feb. 2017.

[17] T. Stojimirovic and C. Renner, "Accuracy of TWR-Based Ranging and Localization in Mobile Acoustic Underwater Networks," in *Fifth Underwater Communications and Networking Conference (UComms)*, Lerici, Italy, Sep. 2021, accepted for publication.

[18] M. Pelka, "Position Calculation with Least Squares based on Distance Measurements," Lübeck University of Applied Sciences, Tech. Rep., 2015.

[19] Navilock, "Datasheet Navilock NL-8001U Micro USB 2.0 Multi GNSS Receiver u-blox 8," https://www.navilock.com/produkt/62573/pdf.html?sprache=en, 2020, accessed: 2020/09/10.

[20] R. J. Urick, *Principles of Underwater Sound 3rd Ed.* Peninsula, 1996.

[21] J. Heitmann, F. Steinmetz, and C. Renner, "Self-Localization of Micro AUVs Using a Low-Power, Low-Cost Acoustic Modem," in *MTS/IEEE OCEANS Conference and Exposition (OCEANS)*, Charleston, SC, USA, Oct. 2018.